Journal of Applied Mathematics, Mechanics and Engineering
https://www.sciltp.com/journals/jamme

Article

Analysis of Multi-Field Influences on a Fiber-Reinforced Thermoelastic Medium Using the Modified Green–Naghdi Theory

Mohamed I.A. Othman *, Samia M. Said and Esraa M. Gamal *

Department of Mathematics, Faculty of Science, Zagazig University, Zagazig P.O. Box 44519, Egypt
* Correspondence: m_i_a_othman@yahoo.com

How To Cite: Othman, M.I.A.; Said, S.M..; Gamal, E.M. Analysis of Multi-Field Influences on a Fiber-Reinforced Thermoelastic Medium Using the Modified Green–Naghdi Theory. *Journal of Applied Mathematics, Mechanics and Engineering* **2026**, *1*(1), 4.

Received: 3 April 2026
Revised: 18 May 2026
Accepted: 23 June 2026
Published: 15 July 2026

Abstract: The main interest of the present article is to dealing with wave extension in a fiber-reinforced thermoelastic solid under the influence of magnetic field and initial stress. The immediate problem is represented via different forms of the Green-Naghdi framework. Analytical expressions of the physical variables are acquire by using new analysis of normal mode with eigenvalue approach technique. Numerical outcomes are shown graphically and the results received are analyzed. The most significant points are highlighted. The outcomes are shown the a notable impact of the magnetic field, initial stress, and fiber-reinforcement on the physical fields. The framework is useful in modeling thermoelastic behavior during laser processing, welding, and additive manufacturing, where rapid heating and cooling induce complex stress fields. Fiber-reinforced thermoelastic models are applicable to biological tissues and biomedical devices, particularly in laser-based therapies and thermal diagnostics where finite-speed heat conduction is significant. Applications include reactor components and containment structures where fiber-reinforced materials experience intense thermal gradients and require accurate prediction of thermoelastic stresses under non-Fourier heat transfer.

Keywords: fiber-reinforced; thermoelastic; magnetic field; different forms of green-naghdi framework; initial stress

1. Introduction

Fiber-reinforced composites are extensively utilized in engineering design due to their superior performance compared to traditional structural materials, particularly in applications where lightweight components must combine high strength and stiffness. The mechanical behavior of these materials can be described using continuum models. A key characteristic of any reinforced concrete element is that its components (concrete and steel) act together as a single unit when both are in the elastic state, meaning there is no relative movement between them. The constitutive equations governing the infinitesimal stress and strain in the linear regime involve five material constants. Xiong and Tian [1] investigated the impact of initial stress on fiber-reinforced thermoelastic porous media. Abouelregal [2] investigated the influence of initial stress on a thick anisotropic fiber-reinforced plate within the framework of fractal thermo-elasticity theory. Othman et al. [3] explored a new model of plane waves in a two-temperature fiber-reinforced thermoelastic medium under the influence of gravity, utilizing a three-phase-lag model. Zenkour [4] addressed the thermal shock problem in a fiber-reinforced anisotropic half-space exposed to a primary magnetic field. Horrigue and Abbas [5] examined how fractional order and thermal relaxation time impact an unbounded fiber-reinforced medium. Fahmy and Almehmadi [6] applied the dual reciprocity boundary element method to analyze rotating functionally graded anisotropic fiber-reinforced magneto-thermoelastic composites. Kalkal et al. [7] investigated the reflection of plane waves in a rotating thermoelastic medium reinforced with fibers, considering the nonlocal effect. Additionally, Othman et al. [8] analyzed the influence of temperature-dependent properties and inclined loading on a fiber-reinforced thermoelastic medium within the framework of the three-phase-lag. Fiber-reinforced thermoelastic models are essential for predicting stress, deformation, and temperature distribution in composite materials used in aerospace, automotive, and marine structures subjected to combined thermal and mechanical loading.

Initial stress has a significant influence on the dynamic and thermal behavior of elastic and thermoelastic media, particularly in systems exposed to preloading, residual stress, or complex boundary conditions. Its presence modifies wave propagation, stability, and deformation characteristics in solids. Othman and Song [9] investigated plane-wave reflection in an elastic half-space subjected to hydrostatic initial stress, while Othman and Atwa [10] extended this analysis to two-dimensional problems of a fibre-reinforced anisotropic thermoelastic medium comparison with the Green-Naghdi theory. Further, Othman and Said [11] studied the effect of rotation on two-dimensional problem of a fibre-reinforced thermoelastic with one relaxation time. Within the framework of the three-phase-lag model, Abo-Dahab et al. [12] examined the reflection of plane waves in a generalized thermoelastic medium incorporating temperature-dependent properties and initial stress. Abd-Alla and Salah [13] considered the influence of initial stress and rotation on a magneto-thermoelastic half-space under a gravity field without energy dissipation. Abouelregal and Rashid [14] focused on the deformation of micropolar materials under Hall current and initial stress within the context of a double-temperature thermoelastic theory involving phase lag and higher-order effects. More recently, Lianngenga et al. [15] explored how initial stress and micropolar couple modulus affect wave reflection in thermoelastic materials with voids. The modified Green–Naghdi theory is particularly applicable to high-speed aerospace components and re-entry vehicles, where heat propagates in a wave-like manner and classical Fourier heat conduction becomes inadequate.

The theory of magneto-thermoelasticity examines how an external magnetic field influences both elastic and thermoelastic deformations in solid bodies. This area of research has gained widespread attention due to its significance in various technological fields, including nuclear engineering, biomedical applications, and geomagnetic exploration. A number of studies [16–25] have applied thermoelastic theories to analyze the impact of magnetic fields on thermoelastic materials. Multi-field thermoelastic analysis supports the design of smart composites incorporating piezoelectric, magneto-thermoelastic, or electro-thermoelastic effects for use in sensors, actuators, and vibration control systems.

The objective of the present work is to analyze the impact of various fields on a fiber-reinforced thermoelastic solid within the framework of the modified Green–Naghdi hypothesis using the eigenvalue approach. Magnetic effects, initial stress, and rein-forcement anisotropy are incorporated into the formulation, and the governing equations are treated through normal mode analysis combined with the eigenvalue method. Analytical solutions are derived for the displacement components, stresses, thermal temperature. Furthermore, a detailed comparison is performed between the considered variables as predicted by generalized thermoelasticity under the modified Green–Naghdi hypothesis and special cases thereof, in both the nonattendance and existence of magnetic field, initial stress, and reinforcement effects. The model is relevant for thermal barrier coatings, insulation layers, and energy conversion devices operating under rapid thermal loading and strong field interactions.

2. Description of the Problem

A problem of a fiber-reinforced magneto-thermoelastic solid in xy - plane under the effect of initial stress was solved. A magnetic field with a invariant intensity $\boldsymbol{H}=(0,0,H_0),$ is playing parallel to the boundary plane (Figure 1). The field equations and fundamental equations can be written like Belfield et al. [26] follows:
The constitutive equations

$$\sigma_{ij}=\lambda e_{kk}\,\delta_{ij}+2\mu_T\,e_{ij}+\alpha(a_k\,a_m\,e_{km}\,\delta_{ij}+a_i\,a_j\,e_{kk})+2(\mu_L-\mu_T)(a_i\,a_k\,e_{kj}+a_j\,a_k\,e_{ki})+\beta\,a_k\,a_m\,e_{km}\,a_i\,a_j$$
$$-\gamma\,\theta\,\delta_{ij}-P(w_{ij}+\delta_{ij}). \tag{1}$$

The equations of motion

$$\rho\,u_{i,tt}=\sigma_{ji,j}+\mu_0\,(\boldsymbol{J}\times\boldsymbol{H})_i\;, \tag{2}$$

$$\mu_0\,(\boldsymbol{J}\times\boldsymbol{H})_1=-\mu_0\,H_0\frac{\partial h}{\partial x}-\varepsilon_0\,\mu_0^2\,H_0^2\frac{\partial^2 u}{\partial t^2},\;\;\mu_0\,(\boldsymbol{J}\times\boldsymbol{H})_2=-\mu_0\,H_0\frac{\partial h}{\partial y}-\varepsilon_0\,\mu_0^2\,H_0^2\frac{\partial^2 v}{\partial t^2},\;\;\mu_0\,(\boldsymbol{J}\times\boldsymbol{H})_3=0. \tag{3}$$

The heat conduction equation

The next unified DPL Green–Naghdi heat conduction equation (Zenkour [27]):

$$K\left(\frac{\partial}{\partial t}+\frac{E K^*}{K}\left(1+\sum_{\ell=1}^{N}\frac{\tau_\theta^\ell}{\ell!}\frac{\partial^\ell}{\partial t^\ell}\right)\right)\nabla^2\theta=\left(1+\sum_{\Lambda=1}^{M}\frac{\tau_q^\Lambda}{\Lambda!}\frac{\partial^\Lambda}{\partial t^\Lambda}\right)\frac{\partial^2}{\partial t^2}(\rho C_E\theta+\gamma T_0 e). \quad (4)$$

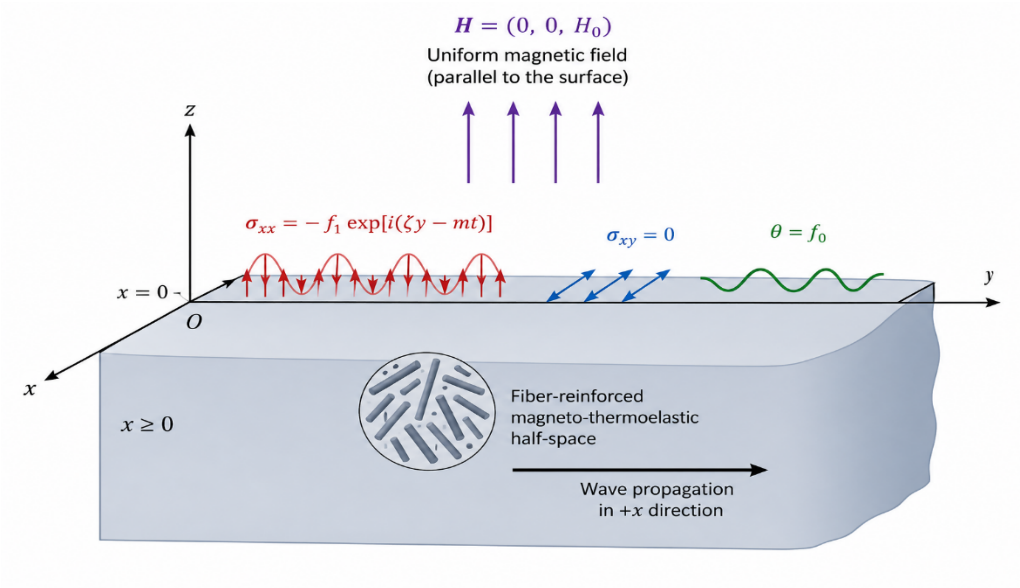

Figure 1. The schematic configuration of the problem.

Some special cases may be obtained from Equation (3), such as:

(a). Equations of the DPL G–N type III model when, $E=1,\ M=N\ge 1$.

(b). Equations of the SPL G–N type III model when, $E=1,\ M=1,\ \tau_\theta=0$.

(c). Equations of the SPL G–N type III model when, $E=0,\ M=1,\ \tau_\theta=0$.

(d). Equations of the G–N type III model when, $E=1,\quad \tau_q=\tau_\theta=0$.

(e). Equations of the G–N type II model when, $E=0,\quad \tau_q=\tau_\theta=0$.

Introducing Equations (1) and (3) into Equation (2), we get

$$\rho\frac{\partial^2 u}{\partial t^2}=A_1\frac{\partial^2 u}{\partial x^2}+A_4\frac{\partial^2 v}{\partial x\partial y}+(\mu_L-\frac{P}{2})\frac{\partial^2 u}{\partial y^2}-\gamma\frac{\partial\theta}{\partial x}-\mu_0 H_0\frac{\partial h}{\partial x}-\varepsilon_0\mu_0^2 H_0^2\frac{\partial^2 u}{\partial t^2}, \quad (5)$$

$$\rho\frac{\partial^2 v}{\partial t^2}=(\mu_L-\frac{P}{2})\frac{\partial^2 v}{\partial x^2}+A_4\frac{\partial^2 u}{\partial x\partial y}+A_3\frac{\partial^2 v}{\partial y^2}-\gamma\frac{\partial\theta}{\partial y}-\mu_0 H_0\frac{\partial h}{\partial y}-\varepsilon_0\mu_0^2 H_0^2\frac{\partial^2 v}{\partial t^2}, \quad (6)$$

where, $A_1=\lambda+2\alpha+4\mu_L-2\mu_T+\beta,\ A_2=\lambda+\alpha,\ A_3=\lambda+2\mu_T,\ A_4=\lambda+\alpha+\mu_L+\frac{P}{2}$.

To facilitate the solution, following dimensionless quantities are introduced:

$$(x',y',u',v')=c_0\eta(x,y,u,v),\quad (t',\tau_q',\tau_\theta')=c_0^2\eta(t,\tau_q,\tau_\theta),\quad \theta'=\frac{\gamma\theta}{(\lambda+2\mu_T)},\quad h'=\frac{h}{H_0},\quad \sigma'_{ij}=\frac{\sigma_{ij}}{\mu_T},$$

$$P'=\frac{P}{(\lambda+2\mu_T)},\quad \eta=\frac{\rho C_E}{K^*},\quad c_0^2=\frac{\lambda+2\mu_T}{\rho}. \quad (7)$$

Equations (5)–(4) with aid of (7) recast into the next sort

$$A_5\frac{\partial^2 u}{\partial t^2}=A_6\frac{\partial^2 u}{\partial x^2}+A_7\frac{\partial^2 v}{\partial x\partial y}+A_8\frac{\partial^2 u}{\partial y^2}-\frac{\partial\theta}{\partial x}, \quad (8)$$

$$A_5 \frac{\partial^2 v}{\partial t^2} = A_8 \frac{\partial^2 v}{\partial x^2} + A_7 \frac{\partial^2 u}{\partial x \partial y} + A_9 \frac{\partial^2 v}{\partial y^2} - \frac{\partial \theta}{\partial y}, \tag{9}$$

$$\left(A_{10} \frac{\partial}{\partial t} + A_0 \left(1 + \sum_{\ell=1}^{N} \frac{\tau_\theta^\ell}{\ell!} \frac{\partial^\ell}{\partial t^\ell} \right) \right) \nabla^2 \theta = \left(1 + \sum_{\Lambda=1}^{M} \frac{\tau_q^\Lambda}{\Lambda!} \frac{\partial^\Lambda}{\partial t^\Lambda} \right) \frac{\partial^2}{\partial t^2} (A_{11} \theta + A_{12} e), \tag{10}$$

where $A_5 = 1 + \frac{\varepsilon_0 \mu_0^2 H_0^2}{\rho}$, $A_6 = \frac{A_1 + \mu_0 H_0^3}{\rho c_0^2}$, $A_7 = \frac{A_4 + \mu_0 H_0^3}{\rho c_0^2}$, $A_8 = \frac{\mu_L - \frac{P}{2}}{\rho c_0^2}$, $A_9 = \frac{A_3 + \mu_0 H_0^3}{\rho c_0^2}$, $A_{10} = \frac{K c_0^4 \eta^3 (\lambda + 2\mu_T)}{\gamma}$, $A_{11} = \frac{\rho C_E c_0^4 \eta^2 (\lambda + 2\mu_T)}{\gamma}$, $A_{12} = \gamma T_0 c_0^4 \eta^2$, $A_0 = \frac{E K^* c_0^2 \eta^2 (\lambda + 2\mu_T)}{\gamma}$.

3. The Analytical Method of Normal Mode Analysis

The solution of considered physical fields can be represented in terms of normal mode analysis

$$[u, v, \theta, \sigma_{ij}](x, y, t) = [\bar{u}, \bar{v}, \bar{\theta}, \bar{\sigma}_{ij}](x) \exp(\mathrm{i}\varsigma y - m t). \tag{11}$$

Introducing Equation (11) in (8)–(10), thus we obtain

$$\mathrm{D}^2 \bar{u} = N_{11} \bar{u} + N_{15} \mathrm{D} \bar{v} + N_{16} \mathrm{D} \bar{\theta}, \tag{12}$$

$$\mathrm{D}^2 \bar{v} = N_{22} \bar{v} + N_{23} \bar{\theta} + N_{24} \mathrm{D} \bar{u}, \tag{13}$$

$$\mathrm{D}^2 \bar{\theta} = N_{32} \bar{v} + N_{33} \bar{\theta} + N_{34} \mathrm{D} \bar{u}, \tag{14}$$

where, $N_{11} = \frac{A_8 \varsigma^2 + A_5 m^2}{A_6}$, $N_{15} = \frac{-\mathrm{i}\varsigma A_7}{A_6}$, $N_{16} = \frac{1}{A_6}$, $N_{22} = \frac{A_9 \varsigma^2 + A_5 m^2}{A_8}$, $N_{23} = \frac{\mathrm{i}\varsigma}{A_8}$, $N_{24} = -\frac{\mathrm{i} A_7 \varsigma}{A_8}$, $N_{32} = \frac{\mathrm{i} A_{15} \varsigma}{A_{13}}$, $N_{33} = \frac{A_{14} + A_{13} \varsigma^2}{A_{13}}$, $N_{34} = \frac{A_{15}}{A_{13}}$, $A_{13} = -A_{10} m + A_0 (1 + \sum_{n=1}^{N} \frac{\tau_\theta^\ell}{\ell!} (-m)^\ell)$, $A_{14} = A_{11} m^2 (1 + \sum_{\ell=1}^{N} \frac{\tau_q^\ell}{\ell!} (-m)^\ell)$, $A_{15} = A_{12} m^2 (1 + \sum_{n=1}^{N} \frac{\tau_q^\ell}{\ell!} (-m)^\ell)$.

The scheme of Equations (12)–(14) can be written in a vector-matrix differential equation as Das and Bhakata [28]

$$\mathrm{D} Q(x) = A(\varsigma, m) Q(x), \tag{15}$$

where $Q(x) = [\bar{u}, \bar{v}, \bar{\theta}, \mathrm{D}\bar{u}, \mathrm{D}\bar{v}, \mathrm{D}\bar{\theta}]^T$,

$$A = \begin{bmatrix} 0 & 0 & 0 & 1 & 0 & 0 \\ 0 & 0 & 0 & 0 & 1 & 0 \\ 0 & 0 & 0 & 0 & 0 & 1 \\ N_{11} & 0 & 0 & 0 & N_{15} & N_{16} \\ 0 & N_{22} & N_{23} & N_{24} & 0 & 0 \\ 0 & N_{32} & N_{33} & N_{34} & 0 & 0 \end{bmatrix}. \tag{16}$$

Using the eigenvalue formulation as Das and Bhakata [28], we now continue to solve the vector-matrix differential Equation (15). The characteristic equation of a matrix A is

$$\Gamma^6 - E_1 \Gamma^4 + E_2 \Gamma^2 - E_3 = 0, \tag{17}$$

where, $E_1 = N_{34} N_{16} + N_{15} N_{24} + N_{33} + N_{22} + N_{11}$,

$E_2 = N_{11} N_{22} + N_{11} N_{33} + N_{22} N_{33} - N_{23} N_{32} - N_{23} N_{15} N_{34} + N_{33} N_{15} N_{24} + N_{16} N_{34} N_{22} - N_{24} N_{32} N_{16}$,

$E_3 = N_{11}N_{22}N_{33} - N_{11}N_{32}N_{23}$,

Let $\Gamma_1^2, \Gamma_2^2, \Gamma_3^2$ be the roots Equation (17) with real positive parts. Then all the six roots of the above characteristic equation, which are also the eigenvalues of the matrix A will be of form $\Gamma = \pm\Gamma_1, \pm\Gamma_2, \pm\Gamma_3$. For the eigenvalue Γ of the matrix A, the six eigenvector $\chi = [x_1, x_2, x_3, x_4, x_5, x_6]^T$,

$x_1 = \Gamma_n N_{16}(\Gamma_n^2 - N_{22}) + \Gamma_n N_{15}N_{23}$,

$x_2 = N_{23}(\Gamma_n^2 - N_{11}) + \Gamma_n^2 N_{24}N_{16}$, $x_3 = (\Gamma_n^2 - N_{11})N_{32} + \Gamma_n^2 N_{34}N_{15}$, $x_4 = \Gamma x_1$, $x_5 = \Gamma x_2$, $x_6 = \Gamma x_3$.

To calculate the eigenvector χ_j, $(j = 1,2,3)$ corresponding to the eigenvalue $\pm\Gamma_j$, $(j = 1,2,3)$ we use the following notations:

$$\chi_1 = [\chi]_{\Gamma=\Gamma_1} \quad \chi_2 = [\chi]_{\Gamma=-\Gamma_1} \quad \chi_3 = [\chi]_{\Gamma=\Gamma_2} \quad \chi_4 = [\chi]_{\Gamma=-\Gamma_2} \quad \chi_5 = [\chi]_{\Gamma=\Gamma_3} \quad \chi_6 = [\chi]_{\Gamma=-\Gamma_3}$$

The answer of Equation (15) which is bound as $x \to \infty$, is given by

$$\bar{u}(x) = \sum_{n=1}^{3} R_n \Pi_{1n} \exp(-\Gamma_n x), \tag{18}$$

$$\bar{u}(x) = \sum_{n=1}^{3} R_n \Pi_{1n} \exp(-\Gamma_n x), \tag{19}$$

$$\bar{\theta}(x) = \sum_{n=1}^{3} R_n \Pi_{3n} \exp(-\Gamma_n x), \tag{20}$$

where, $\Pi_{1j} = [x_1]_{\Gamma=-\Gamma_j}$, $\Pi_{2j} = [x_2]_{\Gamma=-\Gamma_j}$, $\Pi_{3j} = [x_3]_{\Gamma=-\Gamma_j}$.

Using Equations (18)–(20), we obtain

$$\bar{\sigma}_{xx}(x) = \sum_{n=1}^{3} R_n \Pi_{4n} e\,\mathrm{xp}(-\Gamma_n x) - \frac{P(\lambda + 2\mu_T)}{\mu_T} \exp(mt - i\varsigma y), \tag{21}$$

$$\bar{\sigma}_{xy}(x) = \sum_{n=1}^{3} R_n \Pi_{5n} \exp(-\Gamma_n x), \tag{22}$$

where, $\Pi_{4n} = \dfrac{1}{\mu_T}[\mathrm{i}\varsigma A_2 \Pi_{1n} - A_3 \Gamma_n \Pi_{2n} - (\lambda + 2\mu_T)\Pi_{3n}]$, $\quad \Pi_{5n} = \dfrac{\mathrm{i}\varsigma(\mu_L - \frac{P}{2})\Pi_{2n} - (\mu_L + \frac{P}{2})\Gamma_n \Pi_{1n}}{\mu_T}$.

4. Application

To find the parameters $R_n(n = 1,2,3)$, we need to consider the following boundary conditions at $x = 0$

(a). Thermal boundary condition that the surface of the half-space is subjected to

$$\theta = f_0. \tag{23}$$

(b). Mechanical boundary condition that the surface to the half-space is subjected mechanical force

$$\sigma_{xx} = -f_1 \exp(\mathrm{i}\varsigma y - mt). \tag{24}$$

(c). Mechanical boundary condition that the surface to the half-space is traction free

$$\sigma_{xy} = 0, \tag{25}$$

where f_0, f_1 are constants.

Using the expressions of the variables considered into the above boundary conditions (Equations (23)–(25)), we can obtain the following equations satisfied with the parameters:

$$\sum_{n=1}^{3} \Pi_{3n} R_n = f_0, \quad \sum_{n=1}^{3} \Pi_{4n} R_n = f_2, \quad \sum_{n=1}^{3} \Pi_{5n} R_n = 0, \tag{26}$$

where $f_2 = \dfrac{P(\lambda + 2\mu_T)}{\mu_T}\exp(mt - \mathrm{i}\varsigma\, y) - f_1$.

After applying the inverse of the matrix method, we have

$$\begin{pmatrix} R_1 \\ R_2 \\ R_3 \end{pmatrix} = \begin{pmatrix} \Pi_{31} & \Pi_{32} & \Pi_{33} \\ \Pi_{41} & \Pi_{42} & \Pi_{43} \\ \Pi_{51} & \Pi_{52} & \Pi_{53} \end{pmatrix}^{-1} \begin{pmatrix} f_0 \\ f_2 \\ 0 \end{pmatrix}. \tag{27}$$

5. Numerical Calculations and Discussion

To explicate the theoretical results received in the above-mentioned section and analyze these via different forms of the modified Green–Naghdi framework, and discuss the impact of the magnetic field, initial stress, and reinforcement on a fiber-reinforced thermoelastic composite, we present some numerical results for the physical constants as Othman et al. [3]:

$\lambda = 7.76\,\mathrm{x}\,10^9\ \mathrm{N.m^{-2}}$, $\mu = 3.86\,\mathrm{x}\,10^9\ \mathrm{N.m^{-2}}$, $\mu_L = 7.86\,\mathrm{x}\,10^9\ \mathrm{N.m^{-2}}$, $\mu_T = 2.86\,\mathrm{x}\,10^9\ \mathrm{N.m^{-2}}$, $\varsigma = 0.3$,

$f_0 = 0.1$, $\varepsilon_0 = 0.93$, $\beta = 2\,\mathrm{x}\,10^9\,\mathrm{N.m^{-2}}$, $K^* = 386\mathrm{w.m^{-1}.K^{-1}.s^{-1}}$, $K = 386\ \mathrm{w.(mk)^{-1}}$, $C_E = 383.1\mathrm{J.(kgk)^{-1}}$,

$\alpha_t = 1.78\,\mathrm{x}10^{-4}\mathrm{k^{-1}}$, $\rho = 7400\ \mathrm{kg.m^{-2}}$, $T_0 = 293\,\mathrm{k}$, $x = -2.5$, $t = 0.01\mathrm{s}$, $f_1 = 0.5$, $\mu_0 = 1$, $m = m_0 + \mathrm{i}\,\xi$,

$m_0 = -0.4$, $\xi = -0.6$, $\tau_q = 0.9\ \mathrm{s}$, $\tau_\theta = 0.8\ \mathrm{s}$, $\alpha = -1.78\,\mathrm{x}10^9\ \mathrm{N.m^{-2}}$.

Figures 2–5 present the comparisons of the vertical displacement v, temperature distribution θ, and the stress components σ_{xx} and σ_{xy} in the existence and non-attendance of a magnetic field, examined within the frameworks of the dual-phase-lag Green–Naghdi type III (DPL G-N type III), Single-phase-lag, Green–Naghdi type III (SPL G-N type III), and classical Green–Naghdi (G–N) type III theories.

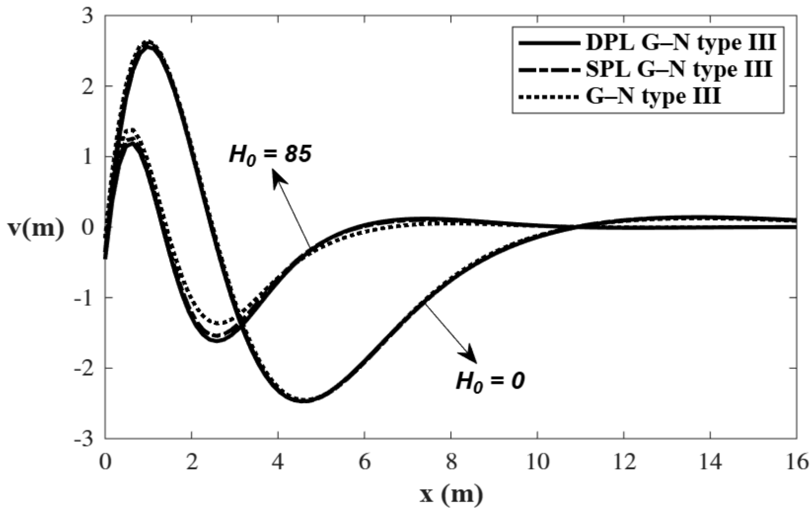

Figure 2. Vertical displacement dispersion v in the attendance and absence of magnetic field.

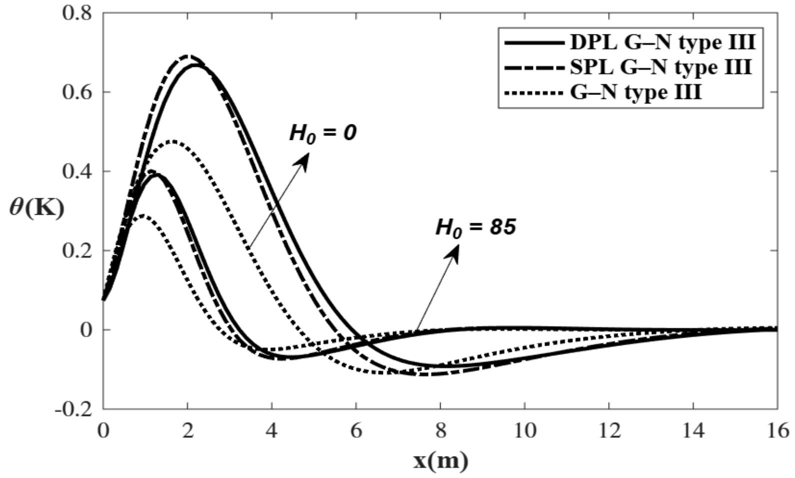

Figure 3. Thermal temperature dispersion θ in the attendance and absence of magnetic field.

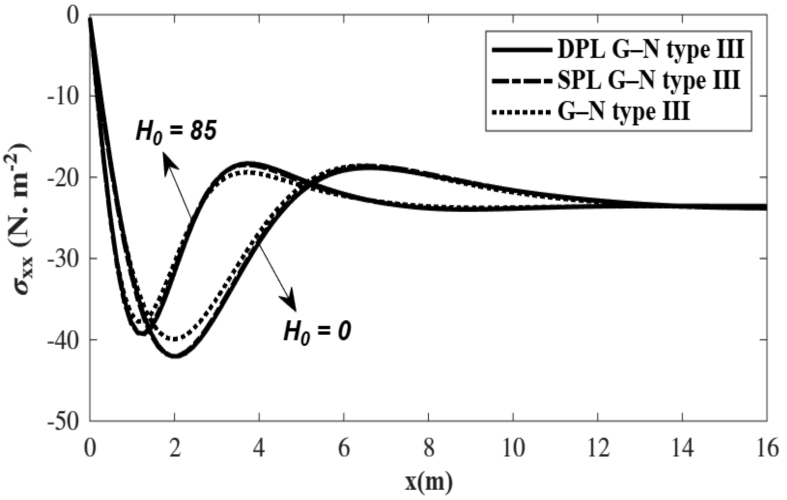

Figure 4. Organization of stress component σ_{xx} in the attendance and absence of magnetic field.

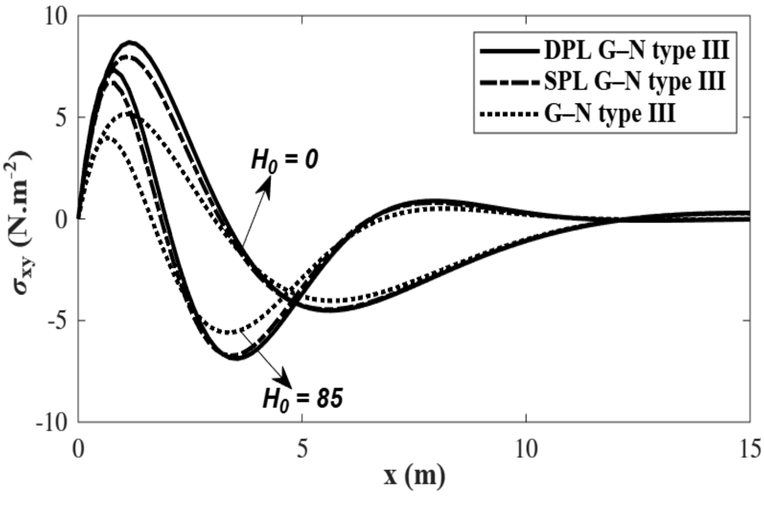

Figure 5. Organization of stress component σ_{xy} in the attendance and absence of magnetic field.

Figure 2 shows that the displacement component v predicted by the DPL, Green–Naghdi Type III model exhibits larger amplitudes than those obtained from the SPL and classical thermoelastic models. This behavior can be attributed to the additional thermal memory effects incorporated in the DPL formulation. Unlike the classical model, where the heat flux responds instantaneously to the temperature gradient, the DPL theory introduces phase lags associated with both the heat flux and the temperature gradient. These relaxation mechanisms delay the thermal response and reduce the effectiveness of thermal diffusion in smoothing spatial temperature variations. The delayed thermal response strengthens the thermoelastic coupling between the temperature and displacement fields. Consequently, a larger portion of the thermal disturbance contributes to mechanical deformation rather than being rapidly dissipated through heat conduction. Furthermore, the Green–Naghdi Type III formulation combines finite-speed thermal-wave propagation with dissipative effects. When augmented by the DPL mechanism, the model retains stronger thermal memory than the SPL and classical formulations, thereby preserving wave energy over a greater distance and producing a stronger dynamic response. Figure 3 shows that the thermal temperature θ increases to a peak value before gradually decaying with distance for both $(H_0 = 0)$ and $(H_0 = 85)$. The DPL, Green–Naghdi Type III model predicts larger temperature amplitudes than the SPL and classical thermoelastic models. This behavior can be attributed to the additional thermal-memory effects introduced by the dual phase-lag formulation. In the classical thermoelastic model, heat conduction follows Fourier's law, which allows thermal disturbances to diffuse rapidly throughout the medium. Consequently, temperature gradients are smoothed quickly, leading to lower peak thermal amplitudes. The SPL model introduces a single relaxation time, which partially delays the thermal response and reduces the rate of heat diffusion. However, the DPL model incorporates two independent phase lags associated with the heat flux and the temperature gradient. As a consequence, thermal energy remains localized for a longer period and is dissipated less rapidly than in the classical and SPL theories. Therefore, the larger values predicted by the DPL, Green–Naghdi Type III model reflect the stronger thermal-memory and energy-storage characteristics introduced by the dual phase lags. The figure also indicates that the thermal response is lower when the magnetic field is present $(H_0 = 85)$. The applied magnetic field generates electromagnetic forces that oppose the motion of charged particles and modify the energy distribution within the medium. Figure 4 shows that the normal stress component σ_{xx} exhibits larger amplitudes in the DPL, Green–Naghdi Type III model compared with the SPL and classical thermoelastic formulations. This difference arises directly from the way thermal disturbances are transported and coupled to mechanical deformation in each theory. In the classical thermoelastic model, Fourier's law governs heat conduction, implying instantaneous thermal diffusion. The SPL model introduces a single thermal relaxation time, which delays the heat flux response and partially preserves thermal gradients. This leads to a moderate increase in stress amplitudes compared with the classical case. In contrast, the DPL, Green–Naghdi Type III model incorporates two phase lags—one associated with the heat flux and another with the temperature gradient. These dual relaxation effects introduce stronger thermal memory and significantly reduce the effective rate of thermal diffusion. Because the normal stress is directly coupled to temperature through the thermoelastic constitutive relation, the persistence of stronger temperature gradients in the DPL model results in larger thermally induced strains. This enhanced thermoelastic coupling amplifies the resulting stress field, producing higher peak values than those observed in the SPL and classical models. Figure 5 shows that the shear stress component σ_{xy} predicted by the DPL, Green–Naghdi Type III model exhibits larger amplitudes than those obtained from the SPL and classical Green–Naghdi formulations, regardless of whether the magnetic field is present. This behavior can be attributed to the enhanced thermal-memory effects introduced by the dual phase-lag mechanism. In the classical model, thermal disturbances are redistributed relatively rapidly throughout the medium, which reduces localized thermal gradients and limits the magnitude of the induced deformation. Consequently, the associated shear stresses remain comparatively small. The SPL model introduces a single thermal relaxation time that delays the thermal response and allows thermal disturbances to persist for longer periods. The DPL, Green–Naghdi Type III model incorporates two independent phase lags corresponding to the heat flux and the temperature gradient. Since shear stress is directly related to gradients of the displacement field, the enhanced spatial nonuniformity produced by the DPL formulation leads to larger shear strains and consequently larger values of σ_{xy}. Therefore, the larger amplitudes observed in the DPL model reflect the stronger thermoelastic coupling and the increased persistence of localized deformation caused by dual phase-lag heat conduction. The Lorentz forces generated by the interaction between induced currents and the applied magnetic field oppose the deformation of the medium and suppress displacement gradients. Consequently, the magnetic field reduces the magnitude of the shear stress and promotes a more rapid decay of the oscillatory response.

Figures 6–9 illustrate the behavior of v, θ, σ_{xx} and σ_{xy} with/without the influence of initial stress. Figure 6 illustrates the variation of the vertical displacement v with the spatial coordinate x in the presence $(P = 5)$ and absence $(P = 0)$ of initial stress. All models exhibit damped oscillatory behavior, indicating wave propagation accompanied by attenuation. The results further show that the introduction of initial stress increases the displacement amplitude, while the DPL, Green–Naghdi Type III model exhibits the largest response, followed by the SPL model and then the classical Green–Naghdi formulation. The amplification caused by the initial stress can be attributed to the modification of the material's pre-stressed state. Initial stress alters the effective stiffness and wave-propagation characteristics of the medium, thereby increasing its susceptibility to thermoelastic disturbances. The stronger response predicted by the DPL, Green–Naghdi Type III model is associated with its dual phase-lag heat-conduction mechanism. Unlike the classical model, where thermal disturbances are redistributed relatively quickly, the DPL formulation introduces two relaxation times that delay the responses of both the heat flux and the temperature gradient. Consequently, the thermoelastic coupling between the temperature field and the displacement field is enhanced. Therefore, the greater sensitivity of the DPL, Green–Naghdi Type III model reflects the combined effect of stronger thermal-memory behavior and enhanced thermoelastic coupling, which amplify the mechanical response of the initially stressed medium. Figure 7 shows that the introduction of initial stress $(P=5)$ increases the thermal response θ, resulting in a higher peak temperature compared with the unstressed case $(P=0)$. The effect is most pronounced in the DPL, Green–Naghdi Type III model, followed by the SPL model, whereas the classical Green–Naghdi model exhibits the smallest thermal response. Consequently, the temperature field exhibits higher peak values than in the stress-free configuration. The larger amplitudes predicted by the DPL, Green–Naghdi Type III model arise from its dual phase-lag heat-conduction mechanism. In the classical formulation, heat conduction redistributes thermal energy relatively rapidly, causing temperature gradients to dissipate quickly and limiting the peak thermal response. The SPL model partially delays this diffusion through a single relaxation time, allowing thermal disturbances to persist for a longer duration. In contrast, the DPL model introduces two independent phase lags associated with the heat flux and the temperature gradient. Therefore, when initial stress enhances the thermoelastic coupling, the DPL formulation is able to retain and amplify the resulting thermal disturbance more effectively than the SPL and classical models. This explains why the DPL, Green–Naghdi Type III model predicts the largest thermal amplitudes among the three theories. Figure 8 shows that the normal stress component σ_{xx} exhibits a damped oscillatory behavior as the spatial coordinate x increases. The presence of initial stress $(P=5)$ significantly increases the magnitude of the compressive stress compared with the unstressed case $(P=0)$. This behavior indicates that the pre-stressed medium stores additional elastic energy, which modifies the wave-propagation characteristics and amplifies the resulting stress field. Among the considered thermo-elastic models, the DPL Green–Naghdi Type III formulation predicts larger stress amplitudes than the SPL and classical models. In the classical formulation, thermal disturbances diffuse more rapidly, causing temperature gradients to dissipate quickly. The SPL model introduces a single relaxation time that delays heat conduction and partially preserves thermal gradients, resulting in moderately larger stress amplitudes. In contrast, the DPL model incorporates two independent phase lags associated with the heat flux and the temperature gradient. Consequently, stronger temperature gradients persist within the medium for longer distances. When combined with the effect of initial stress, which already increases the stored elastic energy in the medium, the DPL formulation produces the largest compressive stress amplitudes among the considered models. Figure 9 shows the variation of the shear stress component σ_{xy} with the spatial coordinate x in the presence and absence of initial stress. In both cases, the response exhibits damped oscillatory behavior, indicating the propagation of coupled thermoelastic waves. Consequently, larger shear strains and higher values of σ_{xy} are generated. The DPL Green–Naghdi Type III model exhibits a stronger response to initial stress than the SPL and classical formulations. As a result, larger displacement gradients develop within the fiber-reinforced medium, producing greater shear strains and consequently larger values of the shear stress component σ_{xy}. Since the DPL model preserves thermal disturbances more effectively than the SPL and classical theories, the influence of the initial stress is amplified to a greater extent, leading to the highest shear-stress amplitudes among the considered models. Therefore, the increased sensitivity of the DPL Green–Naghdi Type III model arises from the combined effects of stronger thermal-memory behavior, enhanced thermoelastic coupling, and the modification of the deformation field induced by the initial stress.

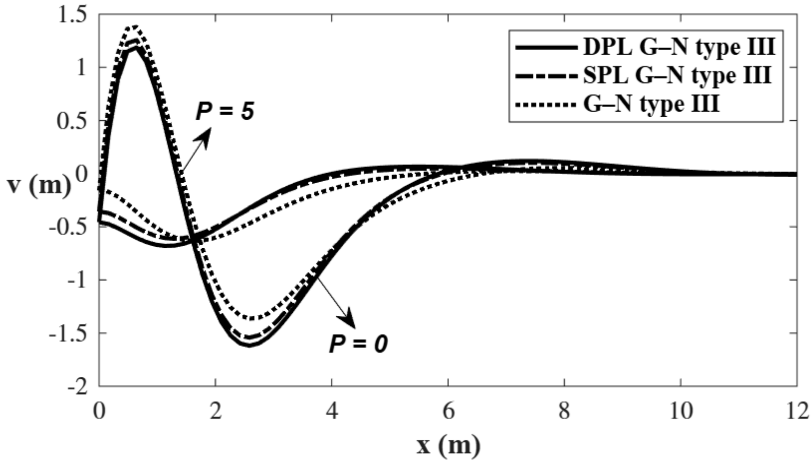

Figure 6. Vertical displacement dispersion v in the attendance and absence of initial stress.

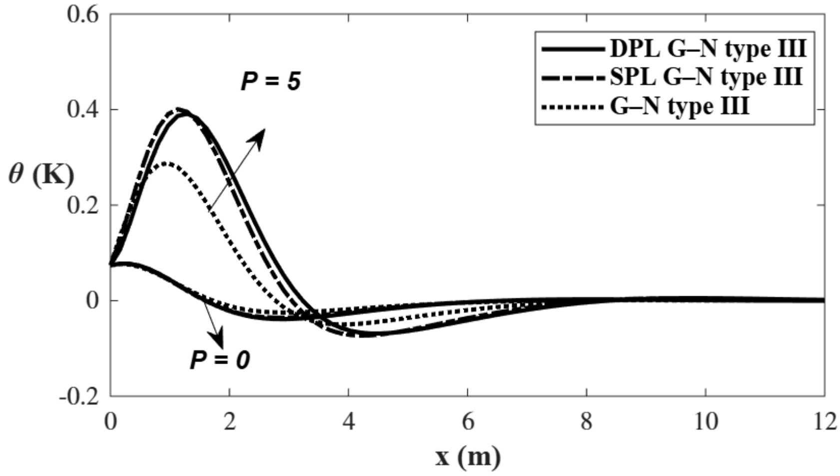

Figure 7. Thermal temperature dispersion θ in the attendance and absence of initial stress.

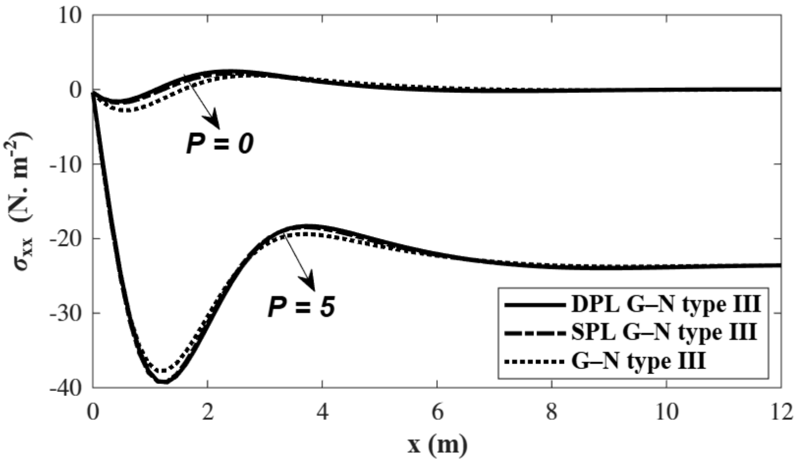

Figure 8. Organization of stress component σ_{xx} in the attendance and absence of initial stress.

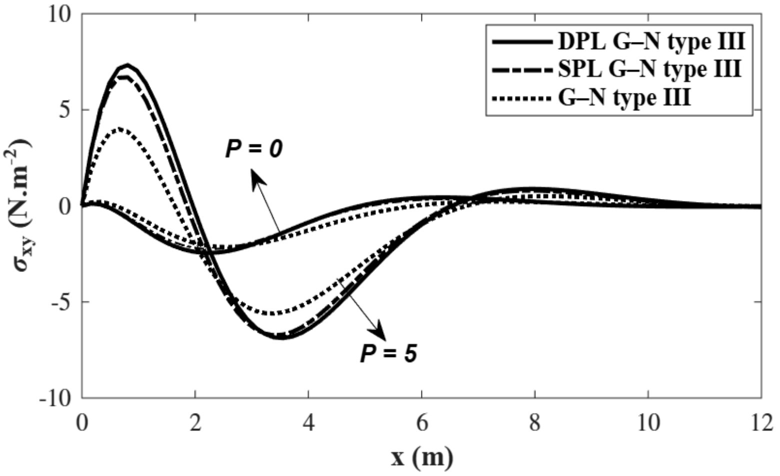

Figure 9. Organization of stress component σ_{xy} in the attendance and absence of initial stress.

Figures 10–13 display the corresponding variations of v, θ, σ_{xx} and σ_{xy} with/without the reinforcement condition. Figure 10 illustrates the variation of the vertical displacement component v, with distance for both reinforced (IRF) and non-reinforced (WRF) media. In all cases, the displacement exhibits an oscillatory wave-like pattern and gradually decays toward zero as the distance increases. The results further indicate that the DPL Green–Naghdi Type III model predicts larger displacement amplitudes than the SPL and classical formulations. Consequently, the induced mechanical displacement remains comparatively small. The SPL model introduces a single thermal relaxation time, which delays heat transport and partially preserves thermal gradients. This strengthens the thermoelastic coupling and leads to larger displacement amplitudes than those predicted by the classical model. The DPL Green–Naghdi Type III model incorporates two independent phase lags corresponding to the heat flux and the temperature gradient. Thus, the enhanced response of the DPL formulation reflects its ability to retain thermal energy and sustain thermoelastic coupling over longer distances. The influence of fiber reinforcement further modifies the displacement field by introducing anisotropy and altering the effective stiffness of the medium. Depending on the reinforcement parameters, the fibers may either constrain or redirect deformation. Figure 11 shows that fiber reinforcement significantly increases the magnitude of the temperature field θ. Among the considered thermoelastic theories, the DPL Green–Naghdi Type III model predicts the largest temperature amplitudes, followed by the SPL model, whereas the classical Green–Naghdi model yields the smallest response. The SPL model introduces a single relaxation time that delays heat transport and partially preserves thermal gradients, thereby increasing the temperature amplitude. The DPL Green–Naghdi Type III model incorporates two independent phase lags associated with the heat flux and the temperature gradient. The presence of reinforcement further promotes the localization of thermo-elastic disturbances. Because the DPL formulation already suppresses thermal diffusion more effectively than the SPL and classical models, the combined effect of reinforcement and dual phase lags results in the strongest retention of thermal energy. Figure 12 illustrates the variation of the normal stress component σ_{xx} with distance x for the DPL Green–Naghdi Type III, SPL Green–Naghdi Type III, and classical Green–Naghdi models. The results show that the presence of fiber reinforcement (IRF) significantly increases the magnitude of the stress response compared with the non-reinforced case (WRF), producing deeper compressive peaks and more pronounced oscillations. The DPL Green–Naghdi Type III model predicts larger stress amplitudes than the SPL and classical formulations because of its enhanced thermal-memory characteristics. In the classical model, thermal disturbances are redistributed relatively quickly, causing temperature gradients to decay rapidly. The SPL model partially delays thermal diffusion through a single relaxation time, allowing stronger temperature gradients and moderately larger stress amplitudes. In contrast, the DPL formulation introduces two independent phase lags associated with the heat flux and the temperature gradient. Consequently, the thermoelastic coupling remains active over a larger spatial region, producing stronger thermally induced strains and larger normal stresses. When combined with the increased stiffness introduced by fiber reinforcement, the enhanced thermal-memory effects of the DPL model generate the largest compressive stress amplitudes among the three theories. Figure 13 illustrates the variation of the shear stress component σ_{xy} with distance x in reinforced (IRF) and non-reinforced (WRF) media. The results show that the non-reinforced medium exhibits larger positive and negative stress peaks, whereas the reinforced medium displays significantly smaller oscillations. Consequently, the material undergoes smaller shear deformations, leading to lower values of the shear stress component σ_{xy}. Among the thermoelastic theories considered, the DPL Green–Naghdi Type III model predicts larger shear-stress amplitudes than the SPL and classical formulations. In the classical model, thermal disturbances diffuse relatively rapidly, reducing the persistence of temperature gradients and weakening the thermoelastic driving forces responsible for deformation. The SPL model partially preserves these gradients through a single relaxation time, resulting in a moderate increase in the stress response. In contrast, the DPL model introduces two phase lags corresponding to the heat flux and the temperature gradient, which significantly enhance thermal-memory effects and reduce the effective rate of thermal diffusion. These gradients generate larger displacement gradients through thermoelastic coupling, leading to greater shear strains and therefore larger values of σ_{xy}.

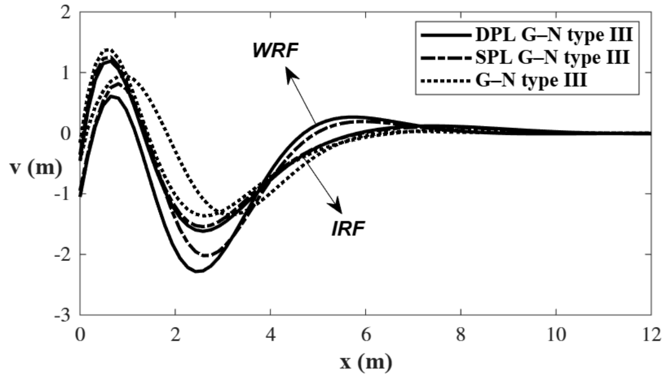

Figure 10. Vertical displacement dispersion v in the attendance and absence of reinforcement.

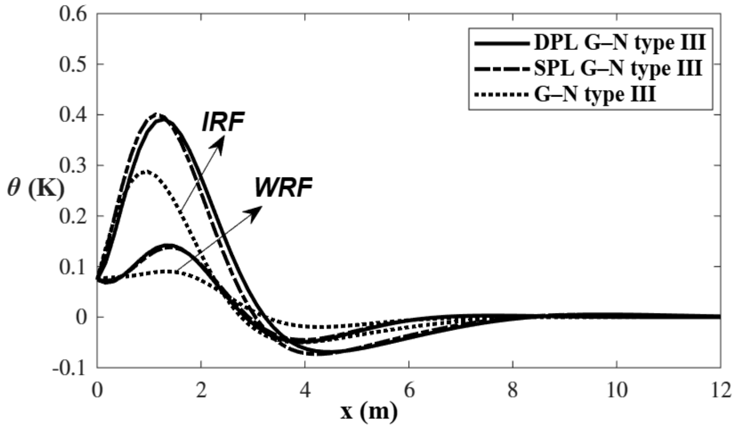

Figure 11. Thermal temperature dispersion θ in the attendance and absence of reinforcement.

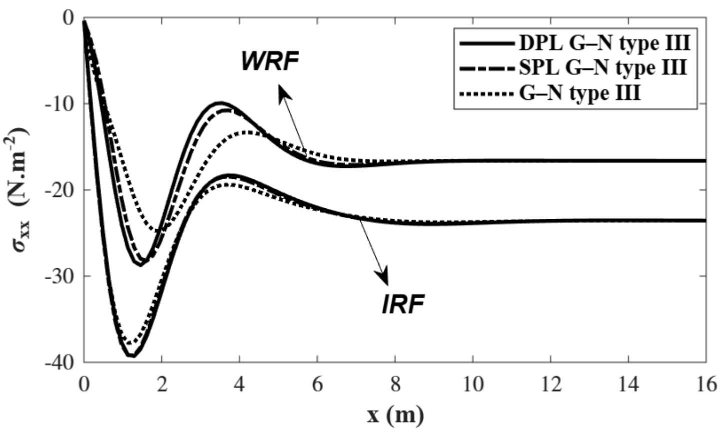

Figure 12. Organization of stress component σ_{xx} in the attendance and absence of reinforcement.

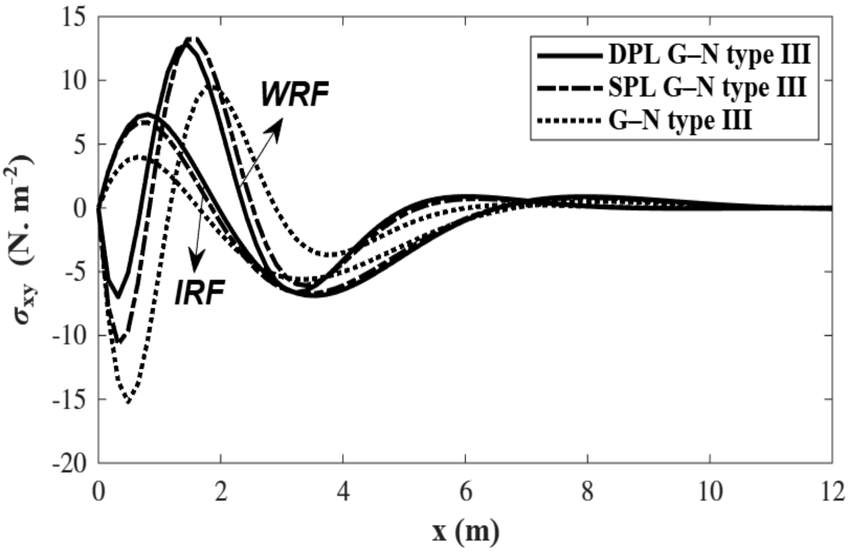

Figure 13. Organization of stress component σ_{xy} in the attendance and absence of reinforcement.

6. Conclusions

In the actual article, we ascertained from graphical outcome, consequence of magnetic field and initial stress in a fiber-reinforced thermoelastic solid, via different forms of the modified Green–Naghdi framework play important role in thermoelasticity field.

We concluded the next remarks:

(a). The impact of initial stress to all physical field play important role in increase and decrease the magnitude these quantities.
(b). It is revealed that various physical fields under consideration are sensitive to reinforcement.
(c). It is found that various physical fields under discussion are sensitive to the magnetic field.
(d). It has been noticed that after reaching maximum and minimum magnitudes, thermoelastic damping becomes linear.
(e). The eigenvalue approach and normal mode analysis used in the current study is applicable to a wide scope of problems in thermodynamics and thermoelasticity.
(f). The thermal relaxation time has fundamental affects on all the physical fields this seemed on examination of the various hypothesis of thermoelasticity in figures.

The outcome bestowed in this study should establish useful for researchers in material science, designers of new materials, physicists as well as for those working on the development of electromagnetic thermoelasticity and in practical situations as in geophysics, optics, acoustics, geomagnetic and oil prospecting etc.

Author Contributions

All authors contributed equally to the conception, editing and proofreading of the manuscript. All authors have read and agreed to the published version of the manuscript.

Funding

This research received no external funding.

Institutional Review Board Statement

Not applicable.

Informed Consent Statement

Not applicable.

Data Availability Statement

The data that support the findings of this study are available from the corresponding author upon reasonable request.

Conflicts of Interest

The authors declare that they have no conflict of interest.

Use of AI and AI-Assisted Technologies

No AI tools were utilized for this paper.

Nomenclature

σ_{ij}	stress tensor
e_{ij}	strain tensor
T	absolute temperature
T_0	temperature in its unbleached state taken, $\left\lvert(\mathrm{T}-T_0)/T_0\right\rvert<1$, $\theta=T-T_0$.
λ,μ	constants of Lame
δ_{ij}	Kronecker's delta
α_t	thermal expansion constant, $\gamma=(3\lambda+2\mu)\alpha_t$
K	coefficient of material constant
K^*	coefficient of thermal conductivity
α, β, $(\mu_L-\mu_T)$	reinforcement parameters
$\boldsymbol{a}\equiv(a_1,a_2,a_3)$,	$a_1^2+a_2^2+a_3^2=1$. We choose the fiber-direction as $\boldsymbol{a}\equiv(1,0,0)$.
$\boldsymbol{u}$	vector of displacement, $\boldsymbol{u}=(u,v,0)$, $\frac{\partial}{\partial z}=0$.
ρ	Density
C_E	specific heat at rigid strain
i	$\mathrm{i}=\sqrt{-1}$
b	wave number
m	complex magnitude
w_{ij}	tensor of rotation, $w_{ij}=\frac{1}{2}(u_{j,i}-u_{i,j})$
$\bar{u}(x)$	physical amplitude of $u(x)$
P	Initial stress
μ_0	magnetic permeability
ε_0	electric permeability
$\boldsymbol{J}$	current density vector
$\dot{\boldsymbol{u}}$	particle velocity of the medium
τ_θ	phase-lag of temperature gradient
τ_q	phase-lag of heat flux.
E	a non-dimensional key number

References

1. Xiong, Q.L.; Tian, X.G. Effect of initial stress on a fiber-reinforced thermoelastic porous media without energy dissipation. *Transp. Porous Media* **2016**, *111*, 81–95.
2. Abouelregal, A.E. Fibre-reinforced generalized anisotropic thick plate with initial stress under the influence of fractional thermoelasticity theory. *Adv. Appl. Math. Mech.* **2017**, *9*, 722–741.
3. Othman, M.I.A.; Said, S.M.; Marin, M. A novel model of plane waves of two-temperature fiber-reinforced thermoelastic medium under the effect of gravity with three-phase lag model. *Int. J. Numer. Methods Heat Fluid Flow* **2019**, *29*, 4788–4806.
4. Zenkour, A.M. Magneto-thermal shock for a fiber-reinforced anisotropic half-space studied with a refined multi-dual-phase-lag model. *J. Phys. Chem. Solids* **2020**, *137*, 109213.
5. Horrigue, S.; Abbas, I.A. Fractional-order thermoelastic wave assessment in a two-dimensional fiber-reinforced anisotropic material. *Mathematics* **2020**, *8*, 1609.
6. Fahmy, M.A.; Almehamdi, M.M. Boundary element analysis of rotating functionally graded anisotropic fiber-reinforced magneto-thermoelastic composites. *Open Eng.* **2022**, *12*, 313–322.

7. Kalkal, K.K.; Deswal, S.; Poonia, R. Reflection of plane waves in a rotating non-local fiber-reinforced transversely isotropic thermoelastic medium. *J. Therm. Stress.* **2023**, *46*, 276–292.
8. Othman, M.I.A.; Said, S.M.; Gamal, E.M.; et al. Modeling temperature-dependent elasticity and diffusion in fiber-reinforced composites under inclined loading. *Iran. J. Sci. Technol. Trans. Mech. Eng.* **2025**, *49*, 2247–2262.
9. Othman, M.I.A.; Song, Y.Q. Reflection of plane waves from an elastic solid half-space under hydrostatic initial stress without energy dissipation. *Int. J. Solids Struct.* **2007**, *44*, 5651–5664.
10. Othman, M.I.A.; Atwa, S.Y. Two-dimensional problems of a fibre-reinforced anisotropic thermoelastic medium comparison with the Green-Naghdi theory. *Comput. Math. Model.* **2013**, *24*, 307–325.
11. Othman, M.I.A.; Saied, S.M. The effect of rotation on two-dimensional problem of a fibre-reinforced thermoelastic with one relaxation time. *Int. J. Thermophys.* **2012**, *33*, 160–171.
12. Abo-Dahab, S.M.; Abd-Alla, A.M.; Othman, M.I.A. Reflection of plane waves on generalized thermoelastic medium under effect of temperature dependent properties and initial stress with three-phase-lag model. *Mech. Based Des. Struct. Mach.* **2020**, *50*, 1184–1197.
13. Abd-Alla, A.M.; Salah, D.M. Effect of initial stress and rotation on magneto-thermoelastic half-space with gravity field and without energy dissipation. *J. Strain Anal. Eng. Des.* **2023**, *59*, 56–66.
14. Abouelregal, A.E.; Rashid, A.F. Deformation in a micropolar material under the influence of Hall current and initial stress fields in the context of a double-temperature thermoelastic theory involving phase lag and higher orders. *Acta Mech.* **2024**, *235*, 4311–4337.
15. Lianngenga, R.; Laldinmawia, T.B.C.; Lalvohbika, J. Effect of initial stress and micropolar couple modulus on the reflection of wave in thermoelastic materials with voids. *J. Vib. Eng. Technol.* **2025**, *13*, 187.
16. Paria, G. Magneto-elasticity and magneto-thermoelasticity. *Adv. Appl. Mech.* **1966**, *10*, 73–112.
17. Sherief, H.H.; Helmy, K.A. A two-dimensional problem for a half-space in magneto-thermoelasticity with thermal relaxation. *Int. J. Eng. Sci.* **2002**, *40*, 587–604.
18. Othman, M.I.A.; Lotfy, K.H. Two-dimensional problem of generalized magneto-thermoelasticity with temperature dependent elastic moduli for different theories. *Multidiscip. Model. Mater. Struct.* **2009**, *5*, 235–242.
19. Said, S.M. Influence of gravity on generalized magneto-thermoelastic medium for three-phase-lag model. *J. Comput. Appl. Math.* **2016**, *291*, 142–157.
20. Sarkar, N.; De, S.; Sarkar, N. Memory response in plane wave reflection in generalized magneto-thermoelasticity. *J. Electromagn. Waves Appl.* **2019**, *33*, 1354–1374.
21. Purkait, P.; Sur, A.; Kanoria, M. Magneto-thermoelastic interaction in a functionally graded medium under gravitational field. *Waves Random Complex Media* **2021**, *31*, 1633–1654.
22. Gupta, S.; Dutta, R.; Das, S.; et al. Double poro-magneto-thermoelastic model with microtemperatures and initial stress under memory-dependent heat transfer. *J. Therm. Stress.* **2023**, *46*, 743–774.
23. Chaudhary, S.; Ahlawat, A.; Panwar, V. Impact of variable thermal conductivity on plane waves between a magneto-thermoelastic medium with Hall current, voids and magneto-thermoelastic medium with Hall current. *Phys. Fluids* **2025**, *37*, 077123.
24. Abbas, I.A.; Marin, M. Analytical solutions of a two-dimensional generalized thermoelastic diffusions problem due to laser pulse. *Iran. J. Sci. Technol. Trans. Mech. Eng.* **2018**, *42*, 57–71.
25. Abouelregal, A.E.; Marin, M.; Öchsner, A. The influence of a non-local Moore-Gibson-Thompson heat transfer model on an underlying thermoelastic material under the model of memory-dependent derivatives. *Contin. Mech. Thermodyn.* **2023**, *35*, 545–562.
26. Belfield, A.J.; Rogers, T.G.; Spencer, A.J.M. Stress in elastic plates reinforced by fiber lying in concentric circles. *J. Mech. Phys. Solids* **1983**, *31*, 25–54.
27. Zenkour, A.M. Thermoelastic diffusion problem for a half-space due to a refined dual-phase-lag Green-Naghdi model. *J. Ocean Eng. Sci.* **2020**, *5*, 214–222.
28. Das, N.C.; Bhakata, P.C. Eigenfunction expansion method to the solution of simultaneous equations and its application in mechanics. *Mech. Res. Commun.* **1985**, *12*, 19–29.